Path Following Control with Slip Compensation on Loose Soil for Exploration Rover

Genya Ishigami, Keiji Nagatani, Kazuya Yoshida

Department of Aerospace Engineering
Tohoku University
Aoba 6-6-01, Sendai, 980-8579, Japan
{ishigami, keiji, yoshida}@astro.mech.tohoku.ac.jp

Abstract— This paper describes a path following control strategy for lunar/planetary exploration rovers taking into account the dynamic behavior, particularly, the slip motion of the rover. It is easily deduced that the slip motion of each wheel of the rover must be increased and not be neglected in case the rover travels on loose soil. Because of the slip, it becomes a difficult task to follow a path. To improve this situation, the authors have developed a path following algorithm with slip compensation. The proposed algorithm can derive both the steering and driving maneuvers for the rover not only to follow an arbitrary path, but also to simultaneously compensate the slip behavior. The performance of our path following strategy is confirmed through our dynamics simulation. The dynamic behavior of the rover in the simulation is calculated using wheel-and-vehicle dynamics model elaborated in our previous research. Also, the slip motion of the wheel is addressed based on a terramechanics approach. The proposed path following control shows better performance than the non-slip controlled one.

I. INTRODUCTION

During the last decade, the progress in the space exploration technology has significantly enabled us to dedicate various scientific missions, such as investigations about the origin of the solar system. Particularly, the effectiveness of a surface exploration robot (*Rover*) in those missions has been demonstrated by NASA's Pathfinder in 1997 [1] and both of Sprit and Opportunity since 2004 [2]. To correspond to a growing demand for more difficult missions, the rover is expected enough to travel much longer distance and climb/traverse slopes. A considerable number of researches have been published from various aspects dealing with the exploration rovers [1]-[5].

The surface of the planetary body, such as the Moon or the Mars, is covered with loose soil, boulders, rocks or stones spread over their terrains. On such challenging terrain, the rover has to plan a better motion path to avoid obstacles autonomously or semi-autonomously, and also precisely navigates itself through the desired path. However, because of wheel slips of the rover on loose soil, it is deduced that the rover hardly follows a given path. Thus, in order to deal with a path following problem on loose soil, it is important to address the slip behavior.

There are a great number of papers and books regarding the path following issues [6]-[9]. For example, Rezaei et al. investigated an on-line path following strategy combined with SLAM algorithm for a car-like robot in outdoor environments [8]. Also, Helmick et al. developed a path following algorithm with slip compensation using a visual odometry and a Kalman filter [9]. However, most of them have not been paying attention to the slips, especially, the wheel slips. Then, it is inappropriate to employ the conventional approach to the issue of the path following on loose soil.

To deal with a slipping wheel on loose soil has been studied in the field of "Terramechanics" [10]-[15]. In this field, the analysis of the wheel-soil interaction mechanism and the modeling of the stress distribution underneath the wheel were well investigated [10][11]. Then, Iagnemma et al. applied those terramechanics models to the issues of planetary rovers [12]. The authors have also elaborated a wheel-and-vehicle dynamics model to deal with the traveling characteristics of a planetary rover [13]-[15].

Thus, in this paper, applying our advantages in regard to the dynamic slip motion, a path following control strategy with slip compensation on loose soil is addressed. As previously described, the slip motion of a rover become relatively large on such loose soil. There are mainly three different slip motions: a rover's sideslip and both longitudinal and lateral slips of the wheel. In conventional approaches of path following control, the slip motions are assumed to be negligible. Then, a kinematic and dynamic model of a vehicle also includes less slip behavior. A key issue in this research is the development of a control strategy that is able to compensate those three slips in order to follow an arbitrary path even on loose soil. We address nonholonomic constrains of the rover considering the lateral slip. And then, while dealing with the path following control, reducing the sideslip of the rover is taken into account. The longitudinal slip is also compensated by controlling an angular velocity of each wheel. Therefore, with the proposed algorithm, it is possible to derive both steering and driving maneuvers to compensate the slip at the same time a given path is followed.

The performance of the path following control is confirmed using our dynamics simulation, which consists of two models: one is a rover's dynamics model to calculate the dynamic behavior of the rover; and the other is the wheel-soil contact model based on the terramechanics to properly deal with the slips of the wheel. The wheel-and-vehicle dynamics model has been successfully validated in our past researches [14][15]. According to the simulation results, the proposed algorithm shows better performance than a non-slip controlled one.
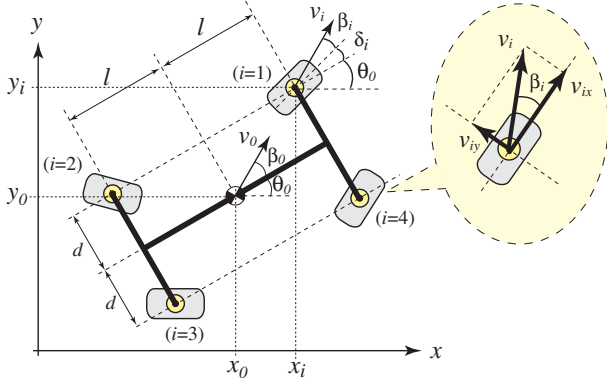
Fig. 1. Kinematics model of 4 wheel vehicle

Particularly, the validity of our control strategy is specifically proved in slope traversing situations.

This paper is organized as follows. Section II describes a nonholonomic kinematic model of a rover with taking into account the slips. In Section III, the proposed path following algorithm is introduced along with a derivation of a desired steering and a driving maneuver, respectively. The dynamics simulation model, which includes the dynamics model of a vehicle and the wheel-soil contact model, is presented in Section IV. In Section V, the simulation study and the performance of the path following control are described.

II. KINEMATIC MODEL OF NONHOLONOMIC VEHICLE

A nonholonomic kinematic model of a vehicle is addressed in this section. The sideslip of the vehicle and lateral slips of the wheels are taken into account while discussing the nonholonomic constraints. Also, an algorithmic singularity for a steering angle derived by a null-space vector of the nonholonomic constraints is introduced.

A. Model assumptions

To discuss a nonholonomic kinematic model of a vehicle, the following assumptions are considered:

1) distances between wheels (generally called as "wheel-base" or "tread") are strictly fixed.
2) the steering axle of each wheel is perpendicular to a surface terrain.
3) a vehicle does not consist of any flexible parts.

B. Kinematic model with slip angle

A kinematic model of a 4 wheel vehicle including the lateral slips is shown in Fig. 1. In this model, each wheel has a certain of steering angle δ_i and slip angle β_i. The slip angle, which defines how large the wheel generates the lateral slip, is calculated by the longitudinal and lateral linear velocities v_{ix}, v_{iy} of the wheel as follows:

$$\beta_i = \tan^{-1}(v_{iy}/v_{ix}) \quad (1)$$

The subscript i denotes each wheel ID as shown in Fig. 1. (x_0, y_0, θ_0) defines a position and an orientation of a center of gravity of the vehicle, while (x_i, y_i) gives a position of each wheel. v_0 and v_i are linear velocity of the vehicle

and each wheel, respectively. Also, β_0 denotes the sideslip of the vehicle, which is determined by the same fashion as equation (1). l means the longitudinal distance from the center of gravity of the vehicle to the front or rear wheels and d defines the lateral distance from the center of gravity of the vehicle to the left or right wheels. Here, based on the assumption as previously pointed, l and d take constant values.

C. Nonholonomic constraints

In the conventional approach, the nonholonomic constrains is discussed with the approximation such as "Bicycle model"[6]. In that model, a four-wheel car-like vehicle is approximated as a two-wheel bicycle-like vehicle. However, the bicycle model is hardly able to deal with the slips of each wheel, strictly. Therefore, with taking into account the slips, the nonholonomic constraints in this research is expressed by:

$$\dot{x}_0 \sin \phi_0 + \dot{y}_0 \cos \phi_0 = 0 \quad (2)$$
$$\dot{x}_i \sin \phi_i + \dot{y}_i \cos \phi_i = 0 \quad (3)$$

where, $\phi_0 = \theta_0 + \beta_0$, and $\phi_i = \theta_0 + \delta_i + \beta_i$. Also, geometric constraints between every wheel and the center of gravity of the vehicle are written as:

$$\left.\begin{array}{l} x_1 = x_0 + l\cos\theta_0 - d\sin\theta_0 \\ x_2 = x_0 - l\cos\theta_0 - d\sin\theta_0 \\ x_3 = x_0 - l\cos\theta_0 + d\sin\theta_0 \\ x_4 = x_0 + l\cos\theta_0 + d\sin\theta_0 \end{array}\right\} \rightarrow x_i = x_0 + X_i \;(4)$$

$$\left.\begin{array}{l} y_1 = y_0 + l\sin\theta_0 + d\cos\theta_0 \\ y_2 = y_0 - l\sin\theta_0 + d\cos\theta_0 \\ y_3 = y_0 - l\sin\theta_0 - d\cos\theta_0 \\ y_4 = y_0 + l\sin\theta_0 - d\cos\theta_0 \end{array}\right\} \rightarrow y_i = y_0 + Y_i \;(5)$$

Substituting equation (4) and (5) into equation (3), the following matrix form equation is obtained:

$$\boldsymbol{A}_0 \cdot \dot{\boldsymbol{q}}_0 = 0 \quad (6)$$

where,

$$\boldsymbol{A}_0 = \begin{bmatrix} \sin\phi_1 & -\cos\phi_1 & -l\cos(\phi_1-\theta_0)-d\sin(\phi_1-\theta_0) \\ \sin\phi_2 & -\cos\phi_2 & l\cos(\phi_2-\theta_0)+d\sin(\phi_2+\theta_0) \\ \sin\phi_3 & -\cos\phi_3 & l\cos(\phi_3-\theta_0)-d\sin(\phi_3+\theta_0) \\ \sin\phi_4 & -\cos\phi_4 & -l\cos(\phi_4-\theta_0)+d\sin(\phi_4-\theta_0) \end{bmatrix}$$

$$\dot{\boldsymbol{q}}_0 = \begin{bmatrix} \dot{x}_0 & \dot{y}_0 & \dot{\theta}_0 \end{bmatrix}^T$$

Here, it is complicated to derive a null-space vector of the constraints matrix $\boldsymbol{A}_0$ if obtaining the vector $\dot{\boldsymbol{q}}_0$ which satisfies equation (6). Therefore, a simplified constrains matrix $\boldsymbol{A}_i$ for each wheel is represented instead of $\boldsymbol{A}_0$.

For instance, in terms of a front-left wheel $(i=1)$:

$$\boldsymbol{A}_1 \cdot \dot{\boldsymbol{q}}_0 = 0 \quad (7)$$

where,

$$\boldsymbol{A}_1 = \begin{bmatrix} \sin\phi_1 & -\cos\phi_1 & -l\cos(\phi_1-\theta_0)-d\sin(\phi_1-\theta_0) \\ \sin\phi_0 & -\cos\phi_0 & 0 \end{bmatrix}$$

Then, using a null-space vector of $\boldsymbol{A_1}$, it is possible to obtain the vector $\dot{\boldsymbol{q}}_0$ satisfying equation (7):

$$\dot{\boldsymbol{q}}_0 = \begin{bmatrix} \cos\phi_0 \\ \sin\phi_0 \\ \frac{\sin(\delta_1+\beta_1-\beta_0)}{-l\cos(\delta_1+\beta_1)-d\sin(\delta_1+\beta_1)} \end{bmatrix} \cdot v \quad (8)$$
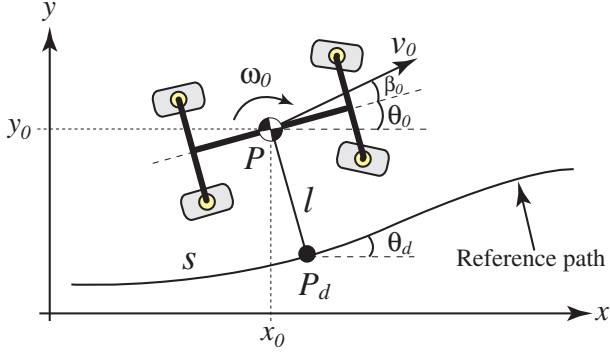
Fig. 2. Illustration of path following control

where, v is an arbitrary velocity, particularly in this case, v can be qualified as a linear velocity of the vehicle, namely v_0. Note that, the above scheme can be formed with respect to the other wheels. Additionally, an algorithmic singularity for a steering angle is calculated from equation (8). The singularity steering angle δ_i^* is derived by paying attention to the denominator of the third component in that equation:

$$\delta_i^* = \pm \tan^{-1}(l/d) - \beta_i \qquad (9)$$

From equation (9), it is reasonable that the singularity steering angle is mainly dominated by the vehicle's configuration, namely l and d. The singularity steering angle gives an unstable state, and then the controllability of the vehicle will become worse.

III. PATH FOLLOWING ALGORITHM WITH SLIP COMPENSATION

In this section, a traditional approach to follow an arbitrary path is recalled, and then a simple strategy to reduce a sideslip of the vehicle is developed. Additionally, we also propose how to distribute the control input to both steering and driving axles with taking into account the slip compensations.

A. Path following control

The following discussion is based on the approach developed in [7]. A general illustration of the path following problem is shown in Fig. 2. The current vehicle's position is denoted by P, the shortest distance projection of P to a reference path is denoted by P_d. Each symbol used in the path following problem is defined as follows:

s : signed curvilinear distance along the path from an initial point to the point P_d.
l : signed distance between P and P_d (distance error.)
θ_d : angle between the x-axis and the tangent to the path at P_d.
c : curvature of the path at P_d.
$\tilde{\theta}$: $= \theta_0 - \theta_d$ is the orientation error.

Using the variables s, l and $\tilde{\theta}$, the kinematic state equations can be formulated as:

$$\left.\begin{array}{rcl} \dot{s} &=& v_0 \cos(\tilde{\theta} + \beta_0)/(1 - c \cdot l) \\ \dot{l} &=& v_0 \sin(\tilde{\theta} + \beta_0) \\ \dot{\tilde{\theta}} &=& \omega_0 - c \cdot v_0 \cos(\tilde{\theta} + \beta_0)/(1 - c \cdot l) \end{array}\right\} \qquad (10)$$

In the path following problem, a feedback control law is required to satisfy both $l \to 0$ and $\tilde{\theta} \to 0$. Then, this objective is realized by the use of one control variable, which is a turning angular velocity $\omega_0 (= \dot{\theta}_0)$ [7]. Thus, considering a linear state feedback control when v_0 is constant and not be zero, a path following control input u_p is given by:

$$u_p = -k_1 v l - k_2 |v| \tilde{\theta} - k_3 |v| \dot{\tilde{\theta}} \qquad (11)$$

where, k_1, k_2 and k_3 are control gains.

B. Sideslip control

On loose soil, the vehicle has a certain amount of sideslip, which is denoted by the slip angle β_0 in Fig. 2. It is simply deduced that the sideslip phenomenon must lead to an unexpected orientation error in the path following issue. Therefore, we consider that the sideslip can be reduced by another control objective, namely $\beta_0 \to 0$.

Combining with the control input represented in equation (11), another control input u_β, which decreases the sideslip of the vehicle, is modeled as:

$$u_\beta = k_4 \beta_0 + k_5 \omega_0 \qquad (12)$$

These two control inputs, u_p and u_β, are selectively distributed to each steering and driving axle: for example, front wheel pair is controlled to follow a path by u_p, while rear pair compensates the sideslip by u_β.

C. Steering and driving maneuvers with slip compensation

The control inputs has to be distributed into several actuators that are mainly located on steering units and wheel driving units of the vehicle.

1) Steering maneuvers: A Desired steering angle of each wheel δ_{di} is elaborated as follows. First, by transforming the nonholonomic constraints equation (3), we can obtain as:

$$\delta_{di} = \tan^{-1}(\dot{y}_i/\dot{x}_i) - \theta_0 - \beta_i \qquad (13)$$

Substituting equation (4) and (5) into equation (13), δ_{di} is derived by the following equation:

$$\delta_{di} = \tan^{-1}\left[\frac{\dot{y}_{d0} - \dot{Y}_i(\dot{\theta}_d)}{\dot{x}_{d0} - \dot{X}_i(\dot{\theta}_d)}\right] - \theta - \beta_i \qquad (14)$$

where, $\dot{x}_{d0}$ and $\dot{y}_{d0}$ are desired linear velocities to each direction. Also, $\dot{X}_i$ and $\dot{Y}_i$ become a function of $\dot{\theta}_d$, which is desired turning angular velocity of the vehicle. Then, the desired control input to equation (14) are eventually summarized as follows:

$$[\; \dot{x}_{d0} \;\; \dot{y}_{d0} \;\; \dot{\theta}_d \;]^T = [\; v_{d0}\cos\theta_d \;\; v_{d0}\sin\theta_d \;\; u_p(\text{or } u_\beta) \;]^T \qquad (15)$$

where, v_{d0} is a desired linear velocity of the center of gravity of the vehicle. Note that, the desired velocity v_{d0} and the control gains, such as k_1-k_5, has to be chosen as avoiding the singularity steering angle as mentioned in equation (9).

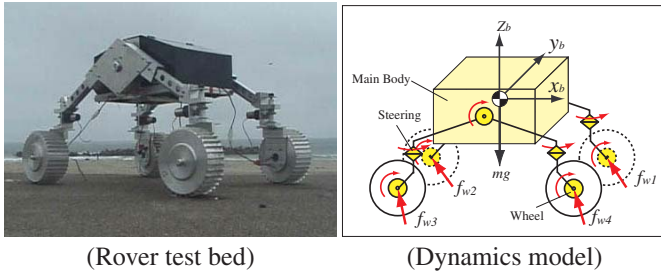(Rover test bed)　　　(Dynamics model)

Fig. 3.　Rover test bed and dynamics model

2) Driving maneuvers: The driving maneuver is implicitly correspond to a control of a wheel angular velocity ω_i. The relationship between ω_i and a wheel linear velocity v_i is written as:

$$\omega_i = v_i \cos \beta_i / r \tag{16}$$

where, r is a wheel radius. On the other hand, v_i can be expressed by $\dot{x}_i$:

$$v_i = \dot{x}_i / \cos \phi_i \tag{17}$$

Based on equation (4), a desired wheel angular velocity ω_{di} is finally derived using $\dot{x}_i = \dot{x}_0 + \dot{X}_i$:

$$\omega_{di} = \frac{\dot{x}_{d0} + \dot{X}_i(\dot{\theta}_d)}{r \cos \phi_i} \cdot \cos \beta_i \tag{18}$$

Additionally, the wheel angular velocity must be adjusted to compensate the longitudinal slip. The slip in the longitudinal direction is defined as the "slip ratio" s_i, which is calculated as a function of the longitudinal linear velocity v_{ix} and the circumference velocity of the wheel $r\omega_i$:

$$s_i = \begin{cases} (r\omega_i - v_{ix})/r\omega_i & (r\omega_i > v_{ix} : \text{driving}) \\ (r\omega_i - v_{ix})/v_{ix} & (r\omega_i < v_{ix} : \text{braking}) \end{cases} \tag{19}$$

The slip ratio takes a value between -1 and 1. Thus, a revised desired angular velocity $\hat{\omega}_{di}$, which compensate the longitudinal slip, is rewritten as follows:

$$\hat{\omega}_{di} = \omega_{di} / (1 - (s_{ref} - s_i)) \tag{20}$$

where, s_{ref} means a reference slip ratio to regulate the longitudinal slip of the wheel. In our approach, the value of s_{ref} is between 0.1 and 0.3, where the traction of the wheel is obtained the most efficient value referring to our past researches.

IV. DYNAMICS MODEL BASED ON TERRAMECHANICS

In this research, in order to confirm the validity of the proposed path following algorithm, the dynamics simulation has been carried out. The dynamics model for the simulation consists of two models: the vehicle's dynamics model and the wheel-soil contact model.
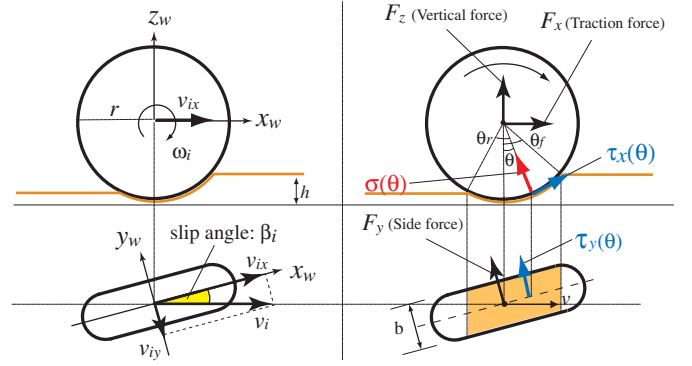

Fig. 4.　Wheel-soil contact model

A. Vehicle Dynamics model

The dynamics model of a vehicle is developed to express the dynamic behavior of the vehicle. The dynamics model of the rover shown in Fig. 3 is completely equivalent to the rover test bed. The dynamic motion equation of the rover is generally written as:

$$H \begin{bmatrix} \dot{\boldsymbol{v}}_0 \\ \dot{\boldsymbol{\omega}}_0 \\ \ddot{\boldsymbol{q}} \end{bmatrix} + C = \begin{bmatrix} \boldsymbol{F}_0 \\ \boldsymbol{N}_0 \\ \boldsymbol{\tau} \end{bmatrix} + J^T \begin{bmatrix} \boldsymbol{F}_e \\ \boldsymbol{N}_e \end{bmatrix} \tag{21}$$

where the symbols used in the above equation are listed as:

$\boldsymbol{H}$　: inertia matrix of the rover.
$\boldsymbol{C}$　: velocity depending term.
$\boldsymbol{v}_0$　: linear velocity of the main body.
$\boldsymbol{\omega}_0$　: angular velocity of the main body.
$\boldsymbol{q}$　: angle of each joint of the rover.
$\boldsymbol{F}_0$　: forces acting at the main body.
$\boldsymbol{N}_0$　: torques acting at the main body.
$\boldsymbol{\tau}$　: torques acting at each joint of the rover.
$\boldsymbol{J}$　: Jacobian matrix.
$\boldsymbol{F}_e$　$= \left[f_{w1}^T, \cdots, f_{wm}^T \right]^T$: external forces acting at each wheel (m is the number of wheels.)
$\boldsymbol{N}_e$　: torques acting at each wheel

Note that, each external force f_{wi} is derived by the wheel-soil contact model, as mentioned in equation (22)-(24) later.

The above equation is general and can be applied to a vehicle with any configurations. Specific parameters for the rover kinematics and dynamics are identified from the test bed and used in the simulation. The motion of the rover with given traveling and steering conditions is numerically calculated by solving the equation (21) successively. The wheel-and-vehicle dynamics model has been successfully validated in our previous researches [14][15].

B. Wheel-soil contact model

The following analysis deals with a rigid wheel traveling on loose soil. A wheel coordinate system is defined as a right-hand frame as shown in Fig. 4, where the longitudinal direction is denoted by x_w, the lateral direction by y_w, and the vertical direction by z_w.

A general force model for a rigid wheel is presented in Fig. 4. Based on the terramechanics approach, wheel contact

forces, such as a traction force F_x, a side force F_y and a vertical force F_z, are able to obtain in the same fashion [10][11][13]:

$$F_x = rb \int_{\theta_r}^{\theta_f} \{\tau_x(\theta)\cos\theta - \sigma(\theta)\sin\theta\}d\theta \quad (22)$$

$$F_y = \int_{\theta_r}^{\theta_f} \{rb \cdot \tau_y(\theta) + R_b \cdot (r - h(\theta)\cos\theta\}d\theta \quad (23)$$

$$F_z = rb \int_{\theta_r}^{\theta_f} \{\tau_x(\theta)\sin\theta + \sigma(\theta)\cos\theta\}d\theta \quad (24)$$

where, b is a width of the wheel, and $\sigma(\theta)$ is the normal stress underneath the wheel. $\tau_x(\theta)$ and $\tau_y(\theta)$ mean shear stresses in the longitudinal and lateral direction of the wheel. Also, the contact region of the wheel on loose soil is determined by the entry angle θ_f and the exit angle θ_r. In addition, R_b is modeled as a reaction resistance generated by the bulldozing phenomenon on a side face of the wheel [13]. R_b is given as a function of a wheel sinkage h.

Note that, σ, τ_x and τ_y are key components to derive the wheel forces, are respectively dominated by the slip ratio and slip angle. The contact region of the wheel is also depended on the slip behavior. Thus, the wheel-soil contact model can deal with the slipping wheel. Through our past researches in [13]-[14], the contact model has been successfully verified.

V. SIMULATION STUDY

The path following simulation was conducted along with comparisons of the performances between the control with and without slip compensations. The vehicle in the simulation is referred to our rover test bed which was developed by the authors, as shown in Fig. 3. The 4-wheeled rover test bed weighs about 35 [kg] in total. The rover has 0.48 [m] in the wheelbase and 0.34 [m] in tread. Each wheel of the rover has an active steering DOF.

The simulations were conducted for mainly two cases; on one, a path following on a horizontal surface, and on the other, on an inclined surface (slope).

A. Simulation procedure

The path following simulation using the wheel-and-vehicle model is executed as follows:

1) Generate a reference path from the initial to the final posture of the vehicle, and define the initial conditions of the simulation.
2) Derive the path following control inputs u_p and u_β using equation (11) and (12).
3) Calculate the desired steering angles δ_{di} and angular velocities $\hat{\omega}_{di}$ based on equation (14) and (20).
4) Calculate the external forces f_{wi} acting to each wheel using the wheel-soil contact model (equation (22)-(24)).
5) Determine $\boldsymbol{F}_0$, $\boldsymbol{N}_0$, $\boldsymbol{F}_e$, $\boldsymbol{N}_e$ and $\boldsymbol{\tau}$.
6) Slove equation (21), then obtain the rover position, orientation and velocities.
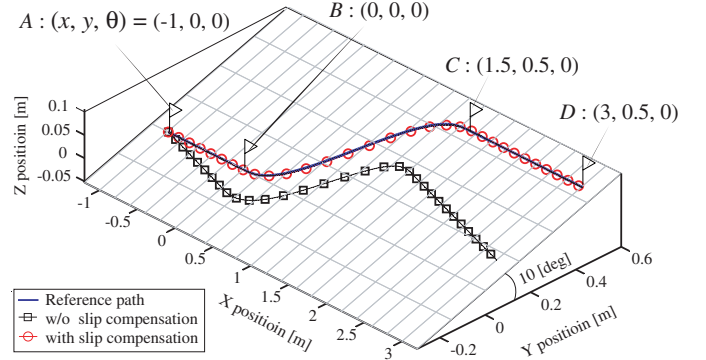7) Calculate the sideslip of the rovre, slip ratios and slip angles of each wheel, then return to step 2).

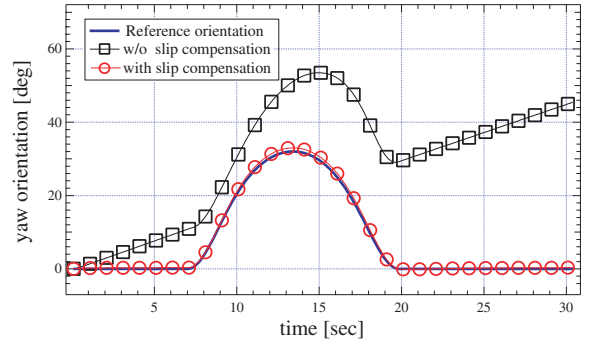Fig. 5. Simulation result in slope case : path following

Fig. 6. Simulation result in slope case : yaw orientation

B. Simulation condition

In both cases of the horizontal and inclined surface, the reference path as shown in Fig. 5 is generated by the following approach: A to B, the reference path is a straight along with the x-axis; B to C, the path is interpolated by a fifth-order polynomial of x; and C to D, the path is defined as a straight path along with the x-axis again. The desired traveling velocity of the rover is given as 0.12 [m/s]. In the case of the inclined surface, a slope angle of the surface is uniformly set as 10 [deg].

In the simulation with the slip compensation, the control input for the path following u_p is distributed into both steering and driving maneuvers on front wheels, while the control input u_β is to the rear wheels to reduce the sideslip.

In case with the non-slip compensated control, the control input u_p is employed into both steering and driving maneuvers of all wheels. Also, the slip ratios s_i and slip angles β_i are assumed to be zero.

C. Simulation result and discussion

In regard to the horizontal case, it is observed that both with and without the slip compensated controls can respectively follow a given path less than 0.5% error. The reasons for the small differences between the both control results are that: 1) the traveling velocity of the rover is relatively small (the value of which is within a general range of a planetary rover); 2) then, less slip behavior is generated while the rover travels. Note that, compensating those slip motions must be necessary
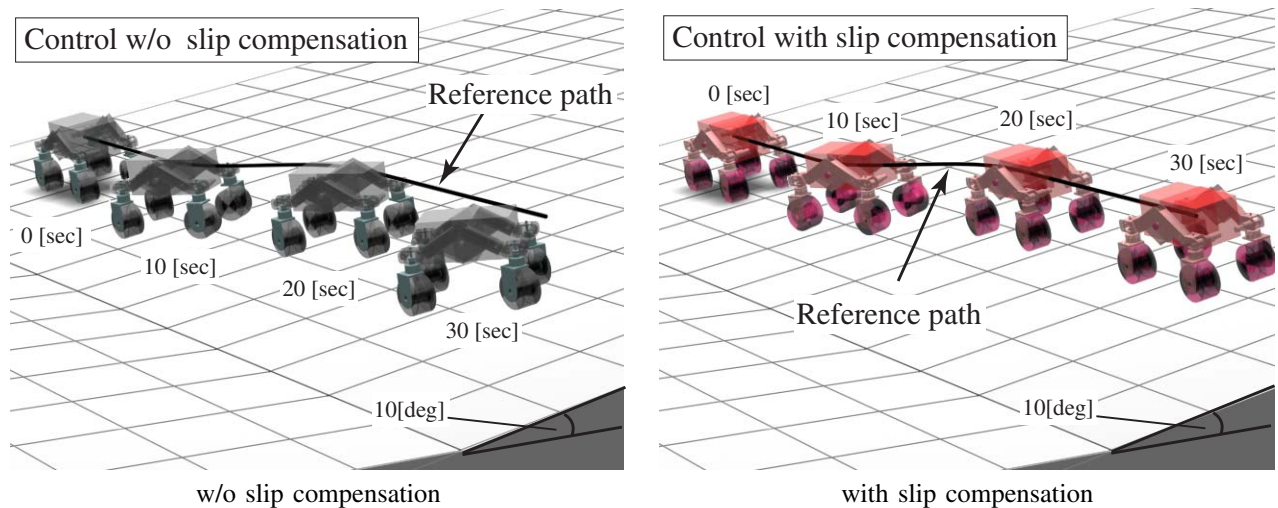
Fig. 7.   Comparison of the rover's behavior on slope

even on horizontal surface if the rover travels with a relatively large velocity as fast as the slip occurs.

The simulation result of the inclined surface regarding the path following is shown in Fig. 5. Also, Fig. 6 describes the time history of the yaw orientation of the rover. From these graphs, it is clearly seen that the control with slip compensation is able to follow the desired path within a negligible error. On the other hand, the result of the control without slip compensation hardly travels along the path since the slip motion of the rover becomes significantly large. In fact, according to the result of the slip behavior, the wheels have around 0.15 in slip ratios and $4 \sim 12$ [deg] in slip angles. Thus, it is proved that the slip compensation control is quite necessary to follow the reference path, particularly on slope traveling situation.

Fig. 7 presents the results of the path following simulation using the computer graphics. It can be seen that the steering maneuvers in the slip compensated control appropriately executes to follow the reference path.

VI. CONCLUSION AND FUTURE WORKS

In this paper, we have addressed the path following control with slip compensation and confirmed the validity of the proposed algorithm along with the dynamics simulation. Through the simulation, the proposed control shows much better performance than the non-slip controlled one. The effectiveness of the slip compensated strategy is especially proved in slope traversing situations.

To apply the control strategy to an actual rover, there are mainly two approaches: One approach is related that the rover is controlled to follow a path based on the proposed algorithm in realtime. However, a key issue in this approach is how to determine the slip ratio and slip angle, specifically, how to monitor the traveling velocity of the rover. Typical techniques to measure the velocity are, for example, to use an accelerometer, to use an IMU (Inertial Measurement Unit), an RTK-GPS (Real Time Kinematic-GPS: if usable even on planetary bodies), or an optical flow method.

The other approach consists that the rover is maneuvered based on a motion profile which was generated from the dynamics simulation in advance. Since, the simulation model described on this paper has been proved to have enough reliability to deal with the actual behavior of a real rover on loose soil.

REFERENCES

[1] http://mars.jpl.nasa.gov/MPF/ (as of February 2006)
[2] http://marsrovers.jpl.nasa.gov/home/index.html (as of February 2006)
[3] I. Nakatani, K. Matsumoto and T. Izumi; "SELENE-B: Proposed Lunar Mission with Lander and Rover," Proc. of the 7th Int. Symp. on Artificial Intelligence, Robotics and Automation in Space, 2003.
[4] R. Volpe and S. Peters; "Rover Technology Development and Infusion for the 2009 Mars Science Laboratory Mission," Proc. of the 7th Int. Symp. on Artificial Intelligence, Robotics and Automation in Space, 2003.
[5] K. Rajan, et. al.; "MAPGEN: Mixed Initiative Planning and Scheduling for the Mars '03 MER Mission," Proc. of the 7th Int. Symp. on Artificial Intelligence, Robotics and Automation in Space, 2003.
[6] A. De Luca, G. Oriolo and C. Samson; "Feedback Control of a Nonholonomic Car-like Robot, *Robot Motion Planning and Control*', edtied by J.-P Laumond, Springer-Verlag, 1998.
[7] C. C. de Wit, H. Khennouf, C. Samson and O. J. Sordalen; "Nonlinear Control Design for Mobile Robots, *Recent Trends in Mobile Robots*," edited by Y. F. Zheng, World Scientific Series in Robotics and Automated Systems, vol.11, 1993.
[8] S. Rezaei, J. Guivant and E. M. Nebot; "Car-Like Robot Path Following in Large Unstructured Environments," Proc of the 2003 IEEE Int. Conf. on Intelligent Robots and Systems, pp. 2468-2473, 2003.
[9] D. M. Helmick et. al.; "Path Following using Visual Odometry for a Mars Rover in High-Slip Environments," Proc. of the 2004 IEEE Aerospace Conference, pp. 772 - 789, 2004.
[10] M. G. Bekker; "Introduction to Terrain-Vehicle Systems," The University of Michigan Press, 1969.
[11] J. Y. Wong; "Theory of Ground Vehicles," John Wiley & Sons, 1978.
[12] K. Iagnemma and S. Dubowsky,; "Mobile Robot in Rough Terrain," Springer Tracts in Advanced Robotics, vol.12, 2004.
[13] K. Yoshida and G. Ishigami; "Steering Characteristics of a Rigid wheel for Exploration on Loose Soil," Proc of the 2004 IEEE Int. Conf. on Intelligent Robots and Systems, pp. 3995–4000, 2004.
[14] G. Ishigami and K. Yoshida ; "Steering Characteristics of an Exploration Rover on Loose Soil Based on All-Wheel Dynamics Model," Proc of the 2005 IEEE Int. Conf. on Intelligent Robots and Systems, pp. 2041-2046, 2005.
[15] G. Ishigami, A. Miwa and K. Yoshida ; "Steering Trajectory Analysis of Planetary Exploration Rovers Based on All-Wheel Dynamics Model," Proc. of the 8th Int. Symp. on Artificial Intelligence, Robotics and Automation in Space, 2005.